Influence of thermal quench on fracture strength, elastic modulus and internal friction of glass plates

CHIN-CHEN CHIU, E. D. CASE
Department of Metallurgy, Mechanics and Materials Science, Michigan State University, East Lansing, MI 48824, USA

The fracture strength and residual stress in glass microscope slides for water, oil and air thermal quenching are compared with the authors' prior theoretical analysis. In addition, elastic modulus and internal friction measurements are used to evaluate the effects of the thermal quenching.

1. Introduction

When a glass plate is quenched from above its annealing temperature, it may acquire thermal shock damage and/or residual stresses [1–5]. The authors have modelled the damage/residual stress state in terms of the transient thermal stress, the fracture strength, the specimen's initial temperature, and the annealing temperature of the glass plate [1]. These variables can be integrated through the thermal shock damage map shown in Fig. 1a [1]. Thermal quench conditions corresponding to the region above the curves cause shock damage. Below the curves, no shock damage occurs. Residual stress develops if the initial glass temperature is above the annealing temperature. From the residual stress, trends in the retained fracture strength of quenched glass can be inferred as in Fig. 1b [1].

Thermal shock damage and residual stresses are typically evaluated via the fracture strength [2–5]. However, the elastic modulus and internal friction can also be useful indicators of microcracks and microstructural change [6–12]. Thus, in this study, fracture strength, elastic modulus and internal friction were used to monitor the effect of thermal quenching on glass plates. In addition, the quenching data were compared with the authors' theoretical analysis [1] summarized in Fig. 1. Glass microscope slides were thermally shocked into room-temperature water, oil and air. Flexural fracture strengths were measured using three-point bending and residual stresses were evaluated using an indentation technique. The elastic modulus and internal friction were measured using a standing-wave resonance technique [13–15].

2. Experimental procedure

Commercial glass microscope slides 7.6 cm × 2.54 cm × 0.12 cm (Cat. No. 48300-036, VWR Scientific Inc., San Francisco) were annealed in air in an electrical furnace at 650 °C for 0.5 h. The specimens then were allowed to cool freely in the furnace. The slides were placed on an aluminosilicate refractory board to prevent viscous deformation during annealing.

The specimens' flexural fracture strength, linear thermal expansion, elastic modulus and internal friction were measured after annealing. Flexural fracture strength was measured in a commercial testing machine with a crosshead speed of 0.1 cm min^{-1} using a three-point bend test fixture with a span of 4.5 cm. The

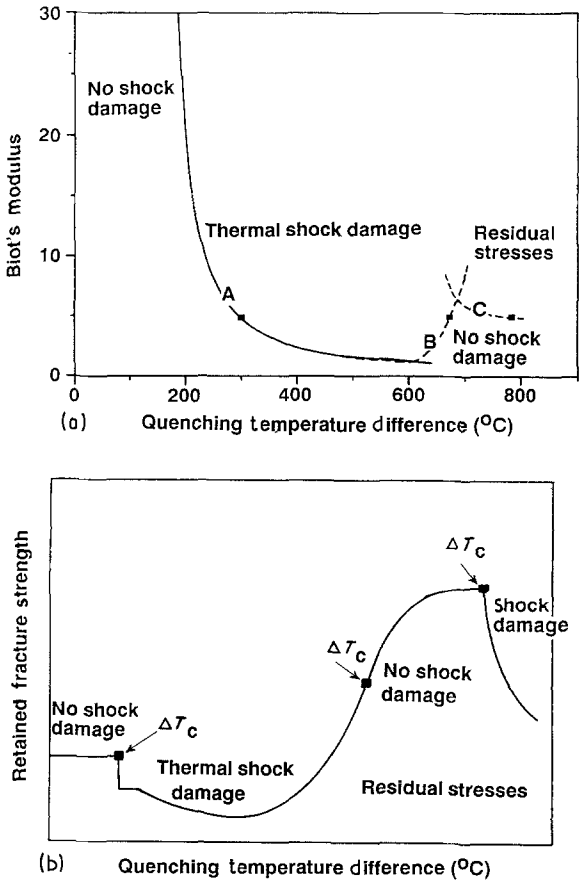

Figure 1 (a) Thermal shock damage map for a glass plate [1]. (b) A schematic diagram of the retained fracture strength of glass plates quenched from above the annealing temperature [1].

0022–2461

fracture strength, σ, was calculated from

$$\sigma = \frac{3PL}{2BD^2} \quad (1)$$

where P is bending load, L is the span between supports, and B, D are the width and the thickness, respectively, of the glass slides.

Linear thermal expansion was measured by a thermomechanical analyser (TMA) (DuPont 9900, DuPont Co., Wilmington, Delaware) at a heating rate of 5 °C min^{-1}. Heat flow as a function of temperature was analysed with a differential scanning calorimeter (DSC) (DuPont 9900) using a heating rate of 10 °C min^{-1} and a nitrogen flow rate of 50 cm^3 min^{-1}.

Elastic moduli were measured by the standing-wave resonance method and internal friction values were measured by the logarithmic decrement technique. Both methods are described elsewhere [13–15].

The annealed slides were heated from room temperature in an electrical furnace. When the furnace temperature was stable for at least 0.5 h, the aluminosilicate refractory board was quickly removed from the furnace for quenching. For the liquid bath quenching, the specimens were dumped into a distilled water bath or a motor oil bath (SAE 20W 50), where the initial temperature of both baths was 20 °C. For air quenching, the slides were quickly set on another cold aluminosilicate board, and again the specimens were allowed to cool freely in air. After the slides reached room temperature, the elastic modulus, internal friction and retained fracture strength were measured. In addition to the room-temperature measurements, the temperature dependence of the elastic modulus was also measured. In order to ensure a statistically reliable estimate of the fracture strength, at least 30 slides were fractured for each quench condition (that is, 30 or more slides were fractured for each quench temperature difference in each of the three quenching media used in this study).

Macro-residual stresses were qualitatively observed by a photoelasticity technique to determine the stress distribution. Residual stresses were measured quantitatively by placing 30 Vickers indentations with a 9.8 N load along the diagonals of both the annealed and quenched slides. The residual stresses on the slide surface were calculated using [16–18]

$$S_r = K_c\left(\frac{4C_r}{\pi}\right)^{-1/2}\left[\left(\frac{C}{C_r}\right)^{3/2} - 1\right] \quad (2)$$

$2C$ and $2C_r$ are the crack lengths at a load of 9.8 N for the annealed and quenched slides, respectively. K_c is the critical stress intensity factor, which is calculated from [19]

$$K_c = 0.016\left(\frac{E}{H}\right)^{1/2}\frac{P}{C^{3/2}} \quad (3a)$$

where E is the elastic modulus of the specimen and P is the indentation load [19]. The hardness H was determined from

$$H = \frac{P}{2a^2} \quad (3b)$$

where $2a$ represents the diagonal length of the indentation impression [19].

3. Results and discussion

3.1. Annealing temperature determination

The linear thermal expansion rate of the glass slides was nearly constant up to 510 °C, but increased sharply for the interval between about 550 and 600 °C (Fig. 2). With further heating the expansion rate decreased as the viscous flow of the glass slides became significant. From Fig. 2, the annealing temperature of the glass was around 550 °C [20].

3.2. Fracture strength

In this study glass plates were quenched into three different media: water, oil, and air. The magnitude of the surface heat transfer coefficient, h, is such that h(water quench) $> h$(oil quench) $> h$(air quench) [21–23]. Thus, the Biot's modulus B is ranked as follows: B(water quench) $> B$(oil quench) $> B$(air quench), where B is defined as [22]

$$B = \frac{rh}{K} \quad (4)$$

Parameters r, h and K are the characteristic specimen dimension, surface heat transfer coefficient and thermal conductivity, respectively.

Typical thermal shock experiments involve quenching only from below the annealing temperature. In this study, we included thermal quenching from both above and below the annealing temperature. This wider range of temperatures is important since the observed retained fracture strength for specimens quenched from below the annealing temperature of 550 °C (for our specimens) can show very different trends from those of specimens quenched from temperatures above the annealing temperature. In addition, the retained fracture strength behaviour depends strongly on the quenching medium. For thermal quenching from below the glass annealing temperature, the retained fracture strength data indicate critical quench

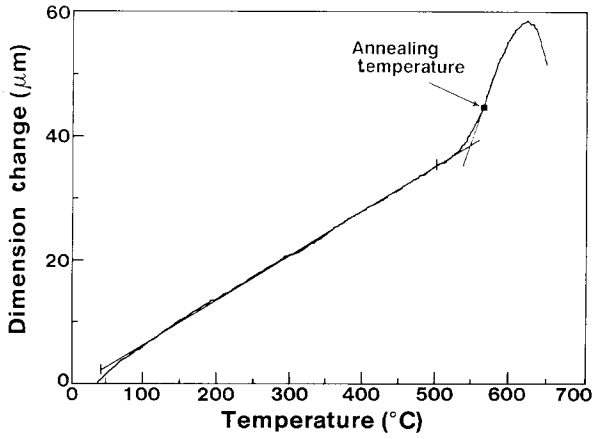

Figure 2 The dimensional change versus temperature for an annealed glass slide, as measured dilatometrically at a heating rate of 5 °C min^{-1}. From about 100 to 500 °C, a nearly constant coefficient of linear thermal expansion of $\alpha = 6.48 \times 10^{-6}$ $°C^{-1}$ was measured.

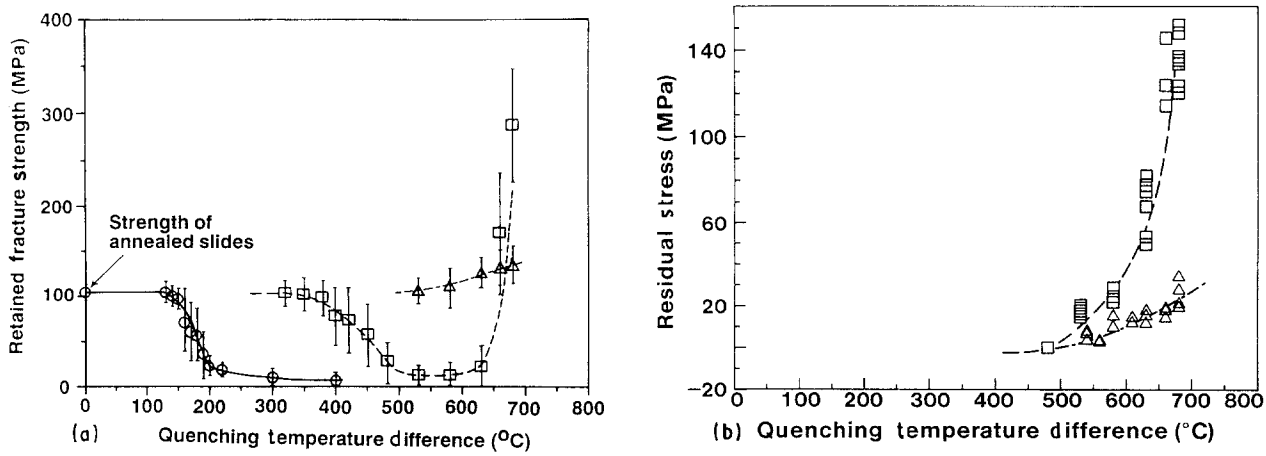

Figure 3 (a) Retained fracture strength of glass slides thermally shocked by (○) water quench, (□) oil quench and (△) air quench as measured in three-point bending. (b) Residual stresses in quenched glass slides determined by Vickers indentation: (□) oil quench, (△) air quench.

temperature differences of $\Delta T_c \approx 165$ and 400 °C for the water quench and oil quench, respectively (Fig. 3a). For air quenching from below the annealing temperature, the retained fracture strength does not change significantly, implying that thermal shock damage does not occur. These experimental results indicate that for thermal quenching from below the glass annealing temperature, a greater Biot's modulus leads to a smaller ΔT_c, which agrees with the authors' previous theoretical analysis (Reference 1 and Fig. 1) and with the thermal shock theories of other researchers such as Kingery *et al.* [23].

The retained fracture strength for quenching from above the annealing temperature is also a function of the quenching medium. Thermal quenching in air from above the annealing temperature results in a retained fracture strength which gradually increases with increasing ΔT. For the oil quench, the retained fracture strength decreases at $\Delta T \approx 400$ °C but increases for $\Delta T > 630$ °C, where the increases in the retained fracture strength result from quench-induced residual stresses [1]. Water quenching always resulted in a drop in residual strength between $\Delta T \approx 165$ and 680 °C. In this study, a maximum ΔT of 680 °C was not exceeded, since for $\Delta T > 680$ °C the specimens deformed macroscopically by viscous flow.

3.3. Thermal quench-induced residual stresses

Indentation measurements [16–18] on quenched glass slide specimens indicate that residual stresses arise in both the oil quench and the air quench for quenching from above the annealing temperature (Fig. 3b). (Residual stress measurements were not attempted on specimens quenched into water from above the annealing temperature, since these specimens cracked extensively.) The oil quench corresponds to a greater Biot's modulus than the air quench, thus the oil quench induces higher residual stresses than the air quench. Although the experimentally determined residual stresses rise very rapidly with increasing ΔT (Fig. 3b), a numerical analysis by the authors [1] predicts that as ΔT continues to rise (for quenching from above the annealing temperature), the residual stress values will level off and saturate with further increases in ΔT. Viscous deformation of the specimens prevented us from determining whether or not a saturation in residual stress does occur for $\Delta T > 680$ °C.

3.4. Effect of thermal quenching on elastic modulus and internal friction

Measurements of elastic modulus and internal friction are non-destructive and reflect the total accumulation of microstructural damage. Figs 4 and 5 illustrate the relationship between elastic modulus, internal friction, and ΔT. As was the case for retained fracture strength, the water quench and oil quench curves change at $\Delta T \approx 165$ and 400 °C, respectively, indicating that thermal shock damage decreases the elastic modulus and increases the internal friction. For the water quench, surface cracks became visible at $\Delta T > 165$ °C, with more and more cracks accumulating as ΔT increased (Fig. 5). Elastic modulus and internal friction continuously vary with increasing ΔT, reflecting an accumulation of cracks. However, the retained strength curves in Fig. 3a are nearly constant despite the accumulation of surface cracks. Analysis of the retained strength behaviour in this case (water quench,

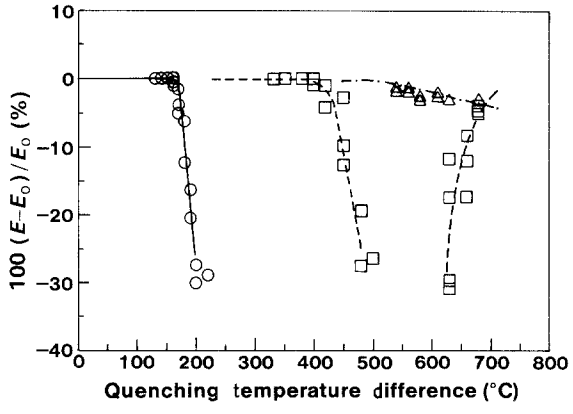

Figure 4 Relative decrease in elastic modulus E as a function of the thermal quench of glass slides: (○) water quench, (□) oil quench, (△) air quench. E_0 is the unquenched elastic modulus.

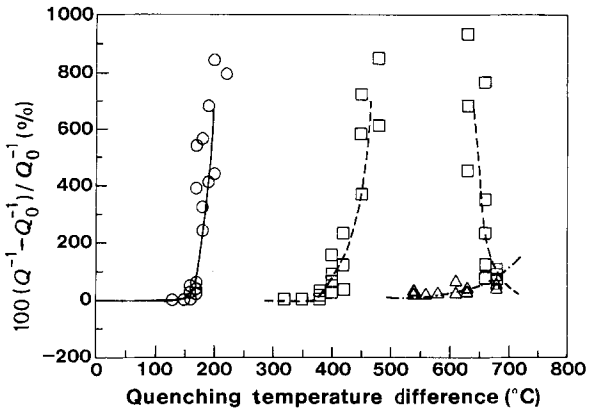

Figure 5 Relative increase in internal friction Q^{-1} as a function of the thermal quench of glass slides: (○) water quench, (□) oil quench, (△) air quench. Q_0^{-1} is the unquenched internal friction.

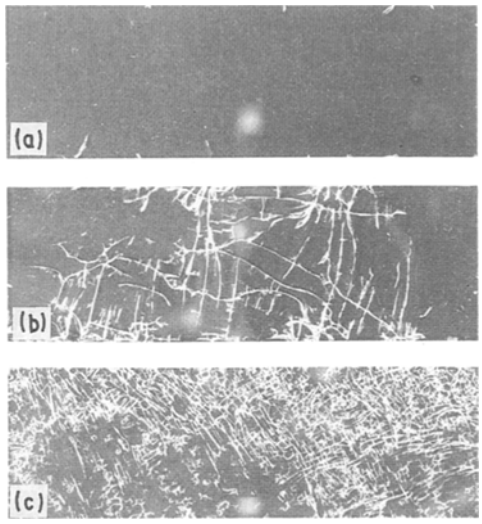

Figure 6 Surface cracks of glass slides quenched into a water bath: ΔT = (a) 180, (b) 230, (c) 400 °C.

$\Delta T > 165$ °C) is very complicated, since the accumulating cracks eventually form a network of cracks. One simple interpretation of the near-constancy in the retained fracture strength is that the critical flaw size does not increase. However, classical fracture mechanics models of isolated, non-interacting cracks in a brittle specimen are likely not to be adequate for the web-like crack field that develops at high ΔT in the water quench (Fig. 6).

The elastic modulus and internal friction are essentially constant for air-quenched specimens (Figs 4 and 5) quenched from below the annealing temperature. Above the annealing temperature, the elastic modulus and internal friction gradually change, and this change may be associated with quench-induced residual stresses (see Appendix A).

Changes in elastic modulus and internal friction as a function of static strain or as a function of thermal quenching have been reported for inorganic and polymer glasses. Mallinder and Proctor [8] indicated that the elastic modulus of soda glass fibre was a function of static strain, $E = E_0(1 - 5.11\varepsilon)$, where $E_0 = 72.5$ Gpa. The strain ε was induced via an external tensile load acting on both ends of a fibre about 0.02 mm in diameter. Vega and Bogue [9] pointed out that thermal quenching into several media caused residual stresses and decreased the elastic modulus of polymer glass (Table I). Pavlushkin *et al.* [10] observed that the elastic modulus of an industrially tempered glass was lower by about 3% than that of annealed glass.* Room-temperature vibrational pendulum measurements in chilled glasses gave an internal friction that was about 40% greater than the internal friction of annealed glass [11, 12].

However, thermal history can affect the specific volume (the reciprocal density), viscosity, and other physical properties of a glass [24, 25]. While thermal quenching does induce residual stress in the glass slides, it is unclear what role (if any) changes in physical properties such as specific volume (that also accompany the thermal quench) play in the observed simultaneous decrease in elastic modulus and increase in internal friction.†

TABLE I Elastic modulus as a function of the quench medium temperature of quenched polymer glass reported by Vega and Bogue [9]

	Temperature of medium (°C)	Modulus (GPa)
Slow cool[a]	30	1.7
Water quench	30	1.5
Slow cool	70	1.5
Water quench[b]	70	0.95
Nitrogen quench	70	1.0

[a] Slow cool = 0.01 °C s^{-1}.
[b] Water quench = 160 °C s^{-1}.

As indicated by Equation 2 (section 2), the quenched-in residual surface stresses in the glass slides were determined as a function of C/C_r, using the Vickers indentation technique [16–18], where $2C$ is the indentation crack length for an annealed specimen and $2C_r$ is the indentation crack length for a residually stressed specimen (indented at a load identical to that used for the annealed slide). Thus, in this study the ratio of C/C_r is used as an index of the severity of thermal quench conditions and residual stresses. The experimentally determined values of residual stress, S_r, ranged from $S_r = 0$ to $S_r = 160$ MPa (Fig. 7). In this study, it was found that the elastic modulus and internal friction percentage changes as a function of quench-induced residual stresses can be expressed as an empirical function of C/C_r (Fig. 7) such that

$$100\left(\frac{E - E_0}{E_0}\right) = -4.35\left[1 - \left(\frac{C}{C_r}\right)^{-9}\right] \quad (5a)$$

$$100\left(\frac{Q^{-1} - Q_0^{-1}}{Q_0^{-1}}\right) = 100\left[1 - \left(\frac{C}{C_r}\right)^{-3}\right] \quad (5b)$$

* Quench temperature and quench media were not specified by Pavlushkin *et al.* [10], Fitzgerald [11], and Day and Rindone [12].
† Thermal quenching results in compressive residual stresses in the specimen's surface. However, the residual stresses do not affect the observed hardness.

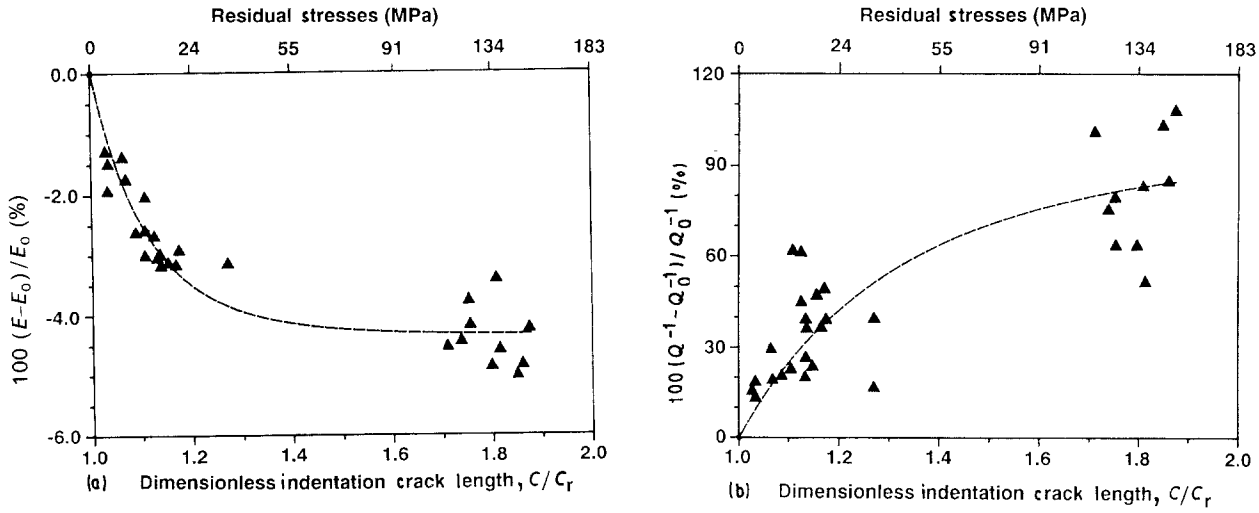

Figure 7 (a) Elastic modulus and (b) internal friction versus thermal quench conditions. The ratio C/C_r is used as an index of the severity of thermal quench conditions and residual stresses (see Equation 2).

where E and Q^{-1} represent the elastic modulus and internal friction, respectively, of the quenched glass slides; E_0 and Q_0^{-1} are the elastic modulus and internal friction of the annealed slides. Since the shock-damage-free specimens with residual stresses of 100 to 40 MPa could not be produced by either motor oil quench (SAE 20W 50) or by air quench (cooling in air), the data in Fig. 7 form two clusters (Appendix B).

3.5. Relaxation of quench-induced residual stresses

Evidence of the relaxation of quench-induced residual stresses can be obtained via both elasticity and calorimetric measurements. While the elastic modulus of an annealed glass slide decreases with temperature, the modulus versus temperature curve for an annealed glass slide is identical upon heating and cooling. The solid line in Fig. 8 shows the reversibility of the elastic modulus for an annealed glass slide heated and cooled at a rate of 1 °C min^{-1}. In contrast, a slide having a quenched-in residual stress does not show reversibility in the elastic modulus for the first heating and cooling cycle. For example, when the annealed glass slide in Fig. 8 was quenched into an oil medium at a quench temperature difference of $\Delta T = 680$ °C, a residual surface stress of 140 MPa was induced in the slide, as measured by the Vickers indentation technique [16–18]. After quenching, room-temperature elasticity measurements on the residually stressed slide showed a lower elastic modulus than the same slide had in its annealed state (Fig. 8). When the residually stressed slide was heated from room temperature to approximately 300 °C (again at a rate of approximately 1 °C min^{-1}), the modulus curve of the quenched slide remained below and approximately parallel to the curve for the annealed state of the slide. Upon heating from 300 °C to a maximum test temperature of 600 °C, the modulus for the residually stressed state of the slide approached the modulus for the annealed state of the slide (Fig. 8). Upon cooling, the modulus of the residually stressed state was slightly above and parallel to the modulus for the initial annealed state. Thus

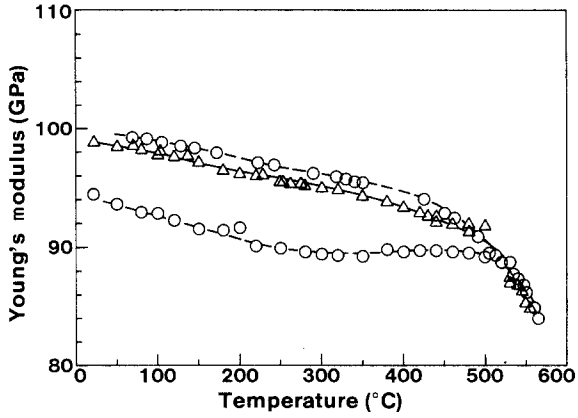

Figure 8 The Young's modulus versus temperature for (△) the annealed state and (○) the residually stressed state of a tempered glass slide.

the heating and cooling curves for the residually stressed state form an open loop (the dashed curves in Fig. 8).

It should be noted that when the heating and cooling cycle was repeated for a second temperature cycle from room temperature to 600 °C and back to room temperature (not shown in Fig. 8), the modulus versus temperature curve was reversible. Thus, the relatively high state of residual stress (140 MPa) apparently did affect the elastic modulus, but (as would be expected) the initial thermal cycling of the specimen from room temperature to 600 °C and back to room temperature at a rate of 1 °C min^{-1} released the residual stresses to the extent that the modulus was reversible upon subsequent thermal cycling at the same heating and cooling rate. Appendix A discusses a model for the experimentally observed change in elastic modulus due to the residual stress state.

Thermodynamically, residual stresses can be regarded as an unstable state, such that when a residually stressed glass plate is heated, the residual stresses are released. The release of the stored elastic strain energy associated with the residual stresses can be examined calorimetrically. Fig. 9 illustrates a DSC analysis of the heat flow as a function of temperature

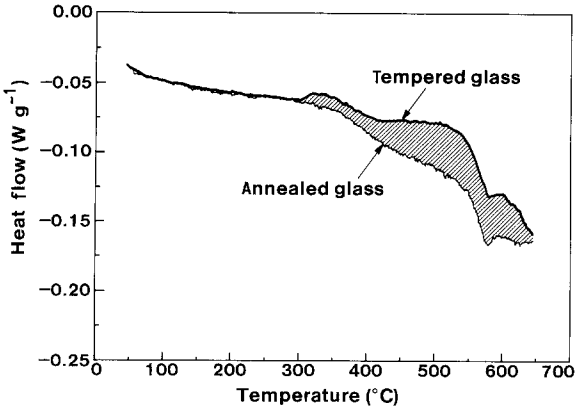

Figure 9 Thermal flow measurement of glass slides using a differential scanning calorimeter.

for the annealed and the residually stressed states of a single glass slide. The annealed and residually stressed states of the glass slide are represented by the solid and dashed lines, respectively. As was the case in the elasticity measurements discussed above, residual stresses in the DSC specimen were induced by a thermal quench of $\Delta T = 680\,^{\circ}C$ into a room-temperature oil bath.

The cross-hatched region between the curves of the annealed and residually stressed states is a measure of the stored elastic strain energy released from the residual stresses in the glass slide. As indicated in Fig. 9, the residual stress relaxation begins at about 350 °C, which roughly agrees with the onset of relaxation indicated by the elastic modulus measurements. However, the DSC measurements were made at a heating rate of $10\,^{\circ}C\,min^{-1}$, while the elasticity measurements were made at a heating and cooling rate of $1\,^{\circ}C\,min^{-1}$. Future studies should repeat the DSC and elasticity measurements on identically treated slides with identical heating and cooling rates during measurement.

4. Conclusions

Thermal quenching into a water bath from below the material's annealing temperature is the standard technique for thermal shock testing of brittle ceramics that behave viscoelastically above some elevated temperature. The typical thermal stress calculations for such experiments are thermoelastic in nature. However, practical thermal stress conditions for a ceramic component may include broad quenching temperature ranges for quenching media other than water, such as an air quench from above the annealing temperature. Consequently, the results of a thermal quench may be the growth of pre-existing cracks and/or the development of thermally-induced residual stresses [1]. The present paper is an experimental study of the thermal quenching of glass microscope slides from below and above the annealing temperature, quenching into three media: air, oil, and water. The study also compares the experimental results with predictions from thermoelastic and thermoviscoelastic calculations [1]. (Thermoviscoelastic theory was required for quenching from above the annealing temperature where viscous flow becomes significant [1].) Both the theoretical analysis [1] and the experimental work (this study) indicate that there are significant differences in the effects of a thermal quench from above the annealing temperature as compared to thermal quenching from below the annealing temperature.

Quenching glass microscope slides may result in thermal shock damage and/or residual stresses depending on the initial temperature, quench temperature difference, and Biot's modulus. Quenching from below the annealing temperature may lead to thermal shock damage. As the Biot's modulus decreases, the critical quench temperature difference increases. Shock damage decreases the retained fracture strength and elastic modulus, while it increases internal friction.

Glass slides quenched from above the annealing temperature exhibit residual stresses which strengthen the slides. The slides are susceptible to thermal shock damage and residual stresses simultaneously when they are quenched from above the annealing temperature. The experimental results indicate that for a given quench temperature difference, a decrease in Biot's modulus (via a change in quench media as discussed in Section 3.2) can reduce the magnitude of the quench-induced residual stress and prevent thermal shock damage. The trend in retained fracture strength data agrees with the present authors' theoretical analysis [1]. Thermal quench from above the annealing temperature, without accompanying thermal shock damage, decreases the elastic modulus and increases internal friction (Appendix A).

Appendix A: Influence of residual stresses on the measurement of the dynamic elastic modulus

Experimental results indicate that thermal quenching of a glass plate from above the annealing temperature can induce residual stresses in the plate and decrease the plate's dynamic resonant frequency (observed as the dynamic elastic modulus, Fig. 8). A qualitative analysis, based on dynamic vibration theory and quench-induced non-linear elasticity, can explain the direct relationship between residual stress development and the resonant frequency decrease.

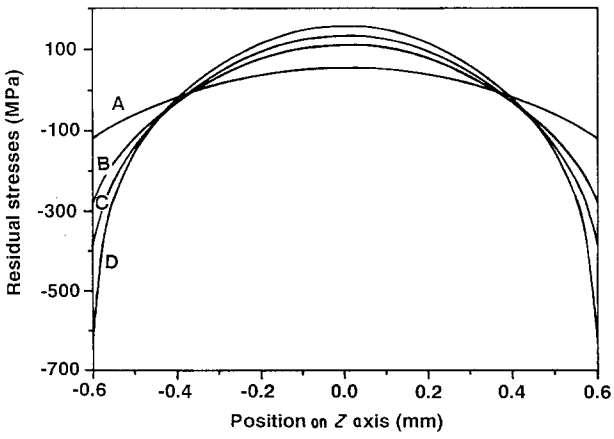

Figure A1 Residual stress profile in a glass plate, as evaluated numerically from thermoviscoelastic theory [1]. $\Delta T = 740\,^{\circ}C$; Biot's modulus = (A) 1, (B) 4, (C) 8, (D) 35.

First, the residual stress profile in tempered glass is determined numerically. Fig. A1 illustrates the stress distribution calculated from thermoviscoelastic stress theory [1]. The residual stress distribution is a complex function of initial glass temperature, thermal quench conditions, etc. However, the spatial distribution is symmetric and nearly parabolic. Therefore, we approximate the stress profile in terms of a polynomial

$$\sigma_*(z) = A_{2n}z^{2n} + A_{2n-2}z^{2n-2} + A_{2n-4}z^{2n-4} + \ldots + A_0 \quad \text{(A1a)}$$

The residual stress σ_* is subject to the boundary conditions

$$\sigma_*(h/2) = \sigma_*(-h/2) < 0 \quad \text{(A1b)}$$

The equilibrium of forces and moments requires that

$$\int_{-h/2}^{h/2} \sigma_*(z)\,dz = 0 \quad \text{(A1c)}$$

$$\int_{-h/2}^{h/2} \sigma_*(z)z\,dz = 0 \quad \text{(A1d)}$$

where σ_* and h represent the quench-induced residual stresses and the thickness of the glass specimen, respectively. In general, a fourth-order polynomial is sufficient to accurately model the residual stress distribution in the glass plates. For example, the calculated residual stress associated with a quench of $\Delta T = 740\,^{\circ}\mathrm{C}$ and Biot's modulus = 15 can be fitted well by $\sigma_*(z) = -1864z^4 - 707z^2 + 134$ (correlation coefficient = 0.997).

Similarly, if we assume a non-linear elasticity similar to that observed by Mallinder and Proctor [8] (section 3.4), the thermal strain distribution, $\varepsilon_*(z)$, can be approximated by the general form

$$\varepsilon_*(z) = B_4z^4 + B_2z^2 + B_0 \quad \text{(A2)}$$

The dynamic elastic modulus of materials may be measured by the standing-wave resonance technique [14–16]. Therefore, we shall model the effect of the residual stress on the dynamic elastic modulus in terms of a free–free suspended vibrating bar. A free–free suspended vibrating bar (Fig. A2) is the test specimen used in the standing resonance technique [14–16].

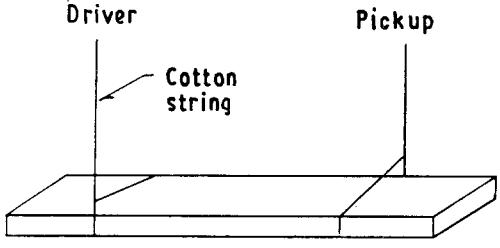

Figure A2 Schematic diagram of specimen suspension for the standing-wave resonance technique of elastic modulus measurement.

According to the dynamics of beams, the governing equation (the Bernoulli–Euler beam equation) is [26]

$$EI\frac{\partial^4 w(x,t)}{\partial x^4} + \left(\frac{a\rho}{g}\right)\frac{\partial^2 w(x,t)}{\partial t^2} = 0 \quad \text{(A3a)}$$

The boundary conditions are

$$\frac{\partial^2 w(0,t)}{\partial x^2} = 0 \qquad \frac{\partial^2 w(L,t)}{\partial x^2} = 0 \quad \text{(A3b)}$$

$$\frac{\partial^3 w(0,t)}{\partial x^3} = 0 \qquad \frac{\partial^3 w(L,t)}{\partial x^3} = 0 \quad \text{(A3c)}$$

where E, ρ, a, L and I represent respectively the elastic modulus, density, cross-sectional area, specimen length, and the second moment of inertia of the cross-section of the beam with respect to the neutral axis. (In this derivation, we neglect the effects of shear deformation and rotary inertia, since their effects are not significant for the bar-shaped specimens considered here [27, 28].) The parameter g is the acceleration due to gravity. w is the transverse deflection of the beam, which is a function of time t and position along the longitudinal axis, x. Solving Equation A3 by separation of variables and applying the boundary conditions gives the characteristic equation [26, 27]

$$w_n(x,t) = w_n(x)[c_1\cos(\beta_n t) + C_2\sin(\beta_n t)] = w_n(x)[C_3\cos(\beta_n t + \theta)] \quad \text{(A4a)}$$

where C_1, C_2, w_n and β_n are defined as

$$\tan\theta = C_2/C_1 \quad \text{(A4b)}$$

$$w_n(x) = \left(\cos(k_nx) + \cosh(k_nx) - \frac{\cos(k_nL) - \cosh(k_nL)}{\sin(k_nL) - \sinh(k_nL)}[\sin(k_nx) + \sinh(k_nx)]\right) \quad \text{(A4c)}$$

$$\beta_n = k_n^2\left(EI\frac{g}{a\rho}\right)^{1/2} \quad \text{(A4d)}$$

and, in addition

$$\cos(k_nL)\cosh(k_nL) = 1 \quad \text{(A4e)}$$

C_1, C_2 and C_3 are integer constants. Each w_n corresponds to the nth mode of the harmonic transverse vibration with the frequency $f_n = \beta_n/2\pi$. For $n = 1$, the fundamental vibrational mode, the first root of Equation A4e is $k_1L = 4.73004$ [26]. Consequently, the fundamental natural frequency of the glass specimen is given by

$$f = \frac{k_1^2}{2\pi}\left(\frac{EI}{a\rho}\right)^{1/2} \quad \text{(A5a)}$$

Furthermore

$$E = \frac{0.09652f^2L^4\rho}{h^2} \quad \text{(A5b)}$$

Equation A5b is useful for elastic modulus calculations of bar-shaped specimens, where E is expressed in terms of $\mathrm{kgf\,m^{-2}}$ ($1\ \mathrm{kgf\,m^{-2}} = 9.806$ Pa).

Experimentally, quenched glass specimens had lower resonance frequencies than the annealed glass specimens. Apparently, residual stresses in the tempered glass lead to the resonant frequency decrease, and from Equation A5b, a decrease in resonant frequency implies a decrease in elastic modulus, E. Equa-

tions A5 (based on linear elasticity) cannot explain the experimentally observed decrease in Young's modulus. On the other hand, the energy method applied to the dynamics of beams (Rayleigh's approximation method) can qualitatively account for the material non-linearity.

Mallinder and Proctor [8] indicated that soda glass exhibits non-linear elasticity under large deformations, such that $E = E_0\ (1 - 5.11\varepsilon)$, where ε is the strain and $E_0 = 72.5$ GPa. Meanwhile, Gogotsi *et al.* [29] and Swain [30] also reported non-linear stress–strain behaviour in ceramic materials. Thus, if we assume that the residual stresses in tempered glass can also induce non-linear effects, namely

$$\begin{aligned} E_* &= E_0\,(1 - C\varepsilon) \\ &= E_0\,[1 - C(\varepsilon_* + \bar{\varepsilon})] \end{aligned} \tag{A6}$$

where ε_* is the thermal residual strain, $\bar{\varepsilon}$ is the longitudinal strain due to beam vibration and C is a proportionality constant. E_0 corresponds to the slope of the stress–strain curve near the origin (Fig. A3). E_* is the elastic modulus as a function of the residual stresses.

In this study, since the flexural deformation of a free–free suspended vibrating bar, $\bar{\varepsilon}$, is small, the geometrical non-linearity is neglected. The deformations of the annealed glass and the tempered glass specimens are assumed to satisfy beam dynamics and classical beam theory. As a result, the observed elastic modulus of an annealed glass bar is $E \approx E_0$. However, residual stresses may lead to non-linear stress–strain behaviour (Fig. A3) so that the natural frequency calculation should include the non-linear elasticity effect.

Mechanical energy conservation requires the maximum kinetic energy to equal the maximum potential energy [28]. Thus,

$$T_{\max} = U_{\max} \tag{A7a}$$

where

$$T = \int_0^L \frac{\rho a}{2g} (\dot{w}_n)^2\,\mathrm{d}x \tag{A7b}$$

$$U = \int_0^L \frac{EI}{2} (w_n'')^2\,\mathrm{d}x \tag{A7c}$$

T and U represent the kinetic energy and the potential energy, respectively, of the annealed glass specimen. $\dot{w}$ and w'' are derivatives with respect to time and x, respectively. From Equation A7 we obtain

$$T = \int_0^L \frac{\rho a}{2g} C_3^2 \beta_n^2 \sin^2(\beta_n t + \theta) w_n^2\,\mathrm{d}x \tag{A8a}$$

$$U = \int_0^L \frac{EI}{2} C_3^2 \cos^2(\beta_n t + \theta) (w'')^2\,\mathrm{d}x \tag{A8b}$$

Equating the maximum values of T and U yields an estimate of f^2, the square of the fundamental natural frequency ($n = 1$) of annealed glass, such that

$$f^2 = \frac{\beta^2}{4\pi^2} = \frac{g \int_0^L EI (w'')^2\,\mathrm{d}x}{4\pi^2 \int_0^L \rho a w^2\,\mathrm{d}x} \tag{A9}$$

Residual stresses change the effective vibrational potential energy in a quenched (tempered) glass bar. However, the functional form of the equation for kinetic energy does not change, and thus Equation A7a is rewritten as

$$T_{\max} = U_{*\max} - U_{*\mathrm{resid}} \tag{A10}$$

$U_{*\max}$ is the maximum potential energy in a tempered glass bar undergoing vibration. $U_{*\max}$ is the sum of the potential energy arising from the internal thermal residual stresses and the longitudinal stress induced by beam vibration (Fig. A3). $U_{*\mathrm{resid}}$ is the thermal residual strain energy of a tempered glass bar in the static or quiescent state. That is, $U_{*\mathrm{resid}}$ is the potential

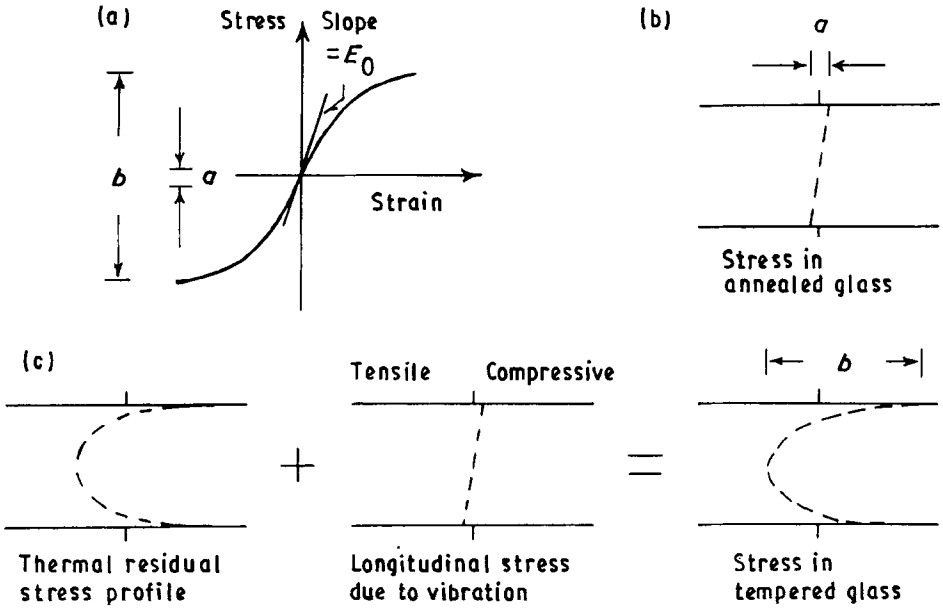

Figure A3 Influence of thermal residual stresses on the stress–strain range of a standing wave. (a) Non-linear stress–strain behaviour of material. (b) Longitudinal stress due to vibration, where a represents the maximum stress–strain range. (c) Superposition of thermal residual stresses and longitudinal stress, where b is the maximum stress–strain range.

energy of the bar when there are no vibrations due to the standing-wave resonance measurement technique. Thus, we have

$$U_{*\max} - U_{*\text{resid}} = b\int_0^L\int_{-h/2}^{h/2}\int[(\sigma_* + \bar{\varepsilon}E_*) - \sigma_*]\,d\varepsilon\,dz\,dx$$

$$= b\int_0^L\int_{-h/2}^{h/2}\int E_0[1 + C(\varepsilon_* + \bar{\varepsilon})]\bar{\varepsilon}\,d\varepsilon\,dz\,dx \quad \text{(A11)}$$

where b is the width of the bar. Combining Equations A2 and A11 yields

$$U_{*\max} - U_{*\text{resid}} = \int_0^L \frac{E_0 I}{2}(w_n'')^2 \times\left[1 - C\left(\frac{3}{112}B_4h^4 + \frac{3}{20}B_2h^2 + B_0\right)\right]dx \quad \text{(A12)}$$

Note that if γ is the curvature of the beam with respect to the neutral axis, then $\varepsilon = z/\gamma$, $1/\gamma = w''$ and $\int\sigma_* z\,dz = 0$. Substituting Equation A12 with Equation A10 and then comparing with Equations A9 and A5b, we get

$$\frac{E_m}{E} = \frac{f_*^2}{f^2} = 1 - C\left(\frac{3}{112}B_4h^4 + \frac{3}{20}B_2h^2 + B_0\right) \quad \text{(A13)}$$

where E_m is the observed elastic modulus. f_* and f are the fundamental natural frequencies of the tempered glass and of the annealed glass, respectively. Equation A13 indicates that, if a tempered glass specimen exhibits non-linear elastic behaviour, the observed elastic modulus may be a function of the residual stress state.

Appendix B: Photoelastic detection of cracks and the subsequent restrictions on quench conditions for crack-free specimens

Photoelasticity is a useful method for detecting the quench-induced cracks in a tempered glass plate. The cracks, which may be (say) 2 mm in length, are sometimes invisible to the unaided eye for specimens quenched from above the annealing temperature, although cracks of a similar length are typically detected much more easily in specimens quenched from below the annealing temperature. The difficulty in detecting cracks in glass slides quenched from above the annealing temperature probably stems from a decrease in crack opening displacement as a function of the surface compressive stresses that arise when glass plates are quenched from above their annealing temperature (Fig. 7a and b).

However, cracks locally disturb the residual stress field of the tempered glass specimens so that photoelastic stress measurements yield fringe patterns that are characteristic of the stress release and redistribution [31, 32]. In the study of the effect of residual stresses on the observed elastic modulus changes (sections 3 and 4), tempered glass specimens were examined photoelastically in order to eliminate the specimens with cracks. By not measuring the elastic modulus for specimens having detectable quench-induced cracks, we attempted to eliminate the crack-modulus effects and focus on the effect of residual stress upon the elastic modulus (see Appendix A also).

For quenching into room-temperature oil (SAE 20W 50), about 1/5 of the specimens quenched at $\Delta T = 680\,^\circ\text{C}$ were eliminated from the elasticity measurement due to cracking, and about 4/5 of the specimens quenched at $\Delta T = 660\,^\circ\text{C}$ were eliminated because of cracking. Oil quenching for the ΔT interval $550\,^\circ\text{C} < \Delta T < 640\,^\circ\text{C}$ did not provide a non-cracked specimen. For an air quench (cooling freely in air), all quenched specimens successfully developed residual stresses without cracking, although due to the lower surface heat transfer coefficient, h, the air quench produced a much lower residual stress than did the oil quench [1]. However, neither quenching route provided specimens with residual stresses, S_r, in the range of $40\text{ MPa} < S_r < 100\text{ MPa}$. Thus, the data in Fig. 7 form two clusters: the cluster of $S_r < 40$ MPa corresponds to the air-quenched specimens, and the cluster where $S_r > 100$ MPa corresponds to the oil-quenched specimens.

References

1. C. C. CHIU and E. D. CASE, *J. Mater. Sci.* **26** (1991) 000.
2. D. P. H. HASSELMAN, R. BADALIANCE, K. R. McKINNEY and E. P. CHEN, *ibid.* **11** (1976) 458.
3. M. ASHIZUKA, T. E. EASLER and R. C. BRADT, *J. Amer. Ceram. Soc.* **66** (1983) 542.
4. H. KAMIZONO and K. NIWA, *J. Mater. Sci. Lett.* **3** (1984) 588.
5. F. V. TOOLEY, "Handbook of Glass Manufacture", Vol. 1 (Ogden, New York, 1961) p. 391.
6. E. D. CASE, *J. Mater. Sci.* **19** (1984) 3702.
7. K. MATSUSHITA, S. KURATANI, T. OKAMOTO and M. SHIMADA, *J. Mater. Sci. Lett.* **3** (1984) 345.
8. F. P. MALLINDER and B. A. PROCTOR, *Phys. Chem. Glasses* **5** (4) (1964) 91.
9. J. D. L. VEGA and D. C. BOGUE, *Chem. Eng. Commun.* **53** (1987) 23.
10. N. M. PAVLUSHKIN, S. I. SILVESTROVICH, V. M. FIRSOV and V. D. KAZAKOV, *J. Mater. Sci.* **4** (1969) 479.
11. J. V. FITZGERALD, *J. Amer. Ceram. Soc.* **34** (1951) 388.
12. D. E. DAY and G. E. RINDONE, *ibid.* **44** (1961) 161.
13. E. SCHREIBER, O. L. ANDERSON and N. SOGA, "Elastic Constants and Their Measurements (McGraw-Hill, New York, 1974) p. 82.
14. J. B. WACHTMAN, *Rev. Sci. Instrum.* **29** (1958) 517.
15. H. M. CHOU and E. D. CASE, *Mater. Sci. Engng* **100** (1988) 7.
16. B. R. LAWN and D. B. MARSHALL, *Phys. Chem. Glasses* **18** (1) (1977) 7.
17. D. B. MARSHALL and B. R. LAWN, *J. Amer. Ceram. Soc.* **60** (1977) 86.
18. *Idem, ibid.* **61** (1978) 21.
19. G. R. ANSTIS, P. CHANTIKUL, B. R. LAWN and D. B. MARSHALL, *ibid.* **64** (1981) 533.
20. R. C. BUCHANAN, "Ceramic Materials for Electronics" (Dekker, New York, 1986) p. 10.
21. R. E. REED-HILL, "Physical Metallurgy Principles", 2nd Edn (Van Nostrand-Reinhold, New York, 1973) p. 704.
22. H. S. CARSLAW and J. C. JAEGER, "Conduction of Heat in Solids" (Clarendon, Oxford, 1959) p. 24.
23. W. D. KINGERY, H. K. BOWEN and D. R. UHLMANN, "Introduction to Ceramics" (Wiley, New York, 1976) p. 822.
24. A. PAUL, "Chemistry of Glasses" (Chapman and Hall, New York, 1982) p. 76.

25. O. S. NARAYANASWAMY, *J. Amer. Ceram. Soc.* **61** (1978) 146.
26. E. VOLTERRA and E. C. ZACHMANOGLOU, "Dynamics of Vibrations" (Merrill Books, Columbus, Ohio, 1965) p. 321.
27. C. C. CHIU and E. D. CASE, *Mater. Sci. Engng*, **A132** (1991) 39.
28. I. H. SHAMES and C. L. DYM, "Energy and Finite Element Methods in Structural Mechanics" (Hemisphere, New York, 1985) p. 334.
29. G. A. GOGOTSI, Y. L. GROUSHEVSKY and K. K STRELOV, *Ceram. Internat.* **4** (1978) 113.
30. M. V. SWAIN, *J. Amer. Ceram. Soc.* **73** (1990) 621.
31. C. W. SMITH, Exper. Mech. **20** (1980) 390.
32. A. SHUKLA and J. W. DALLY, *Ibid.*, **21** (1981) 63.

Received 14 November 1990
and accepted 10 April 1991